THE JOURNAL OF PHYSICAL CHEMISTRY Letters

LETTER

pubs.acs.org/JPCL

Fullerene-Grafted Graphene for Efficient Bulk Heterojunction Polymer Photovoltaic Devices

Dingshan Yu,[†] Kyusoon Park,[‡] Michael Durstock,[§] and Liming Dai*[,†]

[†]Department of Chemical Engineering, Department of Macromolecular Science and Engineering, Case School of Engineering, Case Western Reserve University, Cleveland, Ohio 44106, United States

[‡]Components Technology Group, Advanced R&D Center, LS Mtron Ltd., 555, Hogye-dong, Dongan-gu, Anyang-si, Gyeonggi-do, 431-080 South Korea

[§]Materials and Manufacturing Directorate, Air Force Research Laboratory, RXBP, Wright-Patterson Air Force Base, Ohio 45433, United States

ABSTRACT: A simple lithiation reaction was developed to covalently attach monosubstituted C_{60} onto graphene nanosheets. Detailed spectroscopic (e.g., Fourier transform infrared, Raman) analyses indicated that C_{60} molecules were covalently attached onto the graphene surface through monosubstitution. Transmission electron microscopic (TEM) observation revealed that these monosubstituted C_{60} moieties acted as nucleation centers to promote the formation of C_{60} aggregates of ~5 nm in diameter on the graphene surface. The resultant C_{60}-grafted graphene nanosheets were used as electron acceptors in poly(3-hexylthiophene)-based bulk heterojunction solar cells to significantly improve the electron transport, and hence the overall device performance, yielding a power conversion efficiency of ~1.22%.

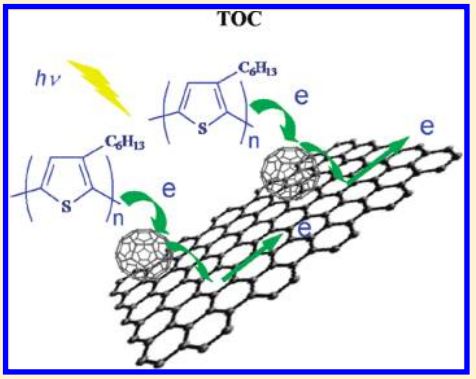

SECTION: Energy Conversion and Storage

Graphene, a new class of two-dimensional (2D) single-atom-thick carbon nanosheets, has attracted significant interest in recent years. Owing to its unique electrical, thermal, and mechanical properties, graphene and its derivatives (e.g., graphene oxide, GO) have been demonstrated to be promising for a variety of potential applications, including nanoelectronics, sensors, nanocomposites, batteries, supercapacitors, and other energy-related devices.[1−13] On the other hand, the large specific surface area intrinsically associated with the 2D graphene sheets offers additional advantages for supporting other nanoentities (such as metal and semiconductor nanoparticles) to form novel hybrid nanostructures with synergetic effects. Examples include graphene−SnO_2 hybrids as anode materials for batteries with improved capacity and cyclic stability,[14] and Pd-decorated graphene electrodes for glucose biosensors with high sensitivity and fast response.[15]

Another allotropic carbon nanostructure, fullerene C_{60}, also possesses certain remarkable physicochemical properties attractive for various optoelectronic applications, particularly as an electron-acceptor in organic photovoltaic cells (PVs).[16] By analogy to the aforementioned graphene and oxide/metal nanoparticle hybrids, the hybridization of graphene with C_{60} is envisioned to create a new class of PV active materials with a strong electron-accepting capability characteristic of C_{60} and good charge transport properties associated with graphene. Indeed, previous studies have shown that C_{60}-decorated carbon nanotubes (CNTs) are promising additives for performance enhancement in polymer PVs.[17] Compared to CNTs, the 2D structure and excellent electronic property of graphene should not only provide a large donor/acceptor interface for efficient charge separation,[18] but also facilitate charge transfer at a low percolation threshold.[19] Therefore, C_{60}−graphene hybrids, if realized, should significantly enhance the performance of polymer solar cells. With little discussion in the literature,[20,21] however, it is still a big challenge to develop facile and efficient synthetic approaches for the construction of C_{60}−graphene hybrids.

As C_{60} is known to readily undergo nucleophilic addition due to its strong electron affinity,[22] we previously attached C_{60} onto 1,4-polydiene chains via the nucleophilic addition reaction involving lithiation of polydiene chains with sec-BuLi, followed by the addition of C_{60} onto the lithiated living polydiene chains.[23,24] In this context, the successful lithiation of single-walled carbon nanotubes (SWCNTs) reported by Ajayan and coworkers[25] assured us to attach C_{60} onto graphene through lithiation of graphene with *n*-BuLi, followed by the addition of C_{60} onto the lithiated graphene via the nucleophilic addition reaction. The introduction of organolithium into the graphitic layer activated it for direct grafting of pristine C_{60} without involving any surfactant[26] (Scheme 1), providing the relatively

Received: March 30, 2011
Accepted: April 18, 2011
Published: April 22, 2011

Scheme 1. Schematic Representation of Grafting C_{60} onto Graphene through Lithiation Reaction with *n*-Butyllithium

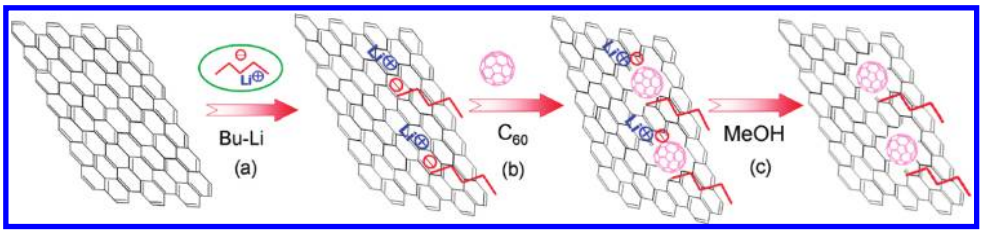

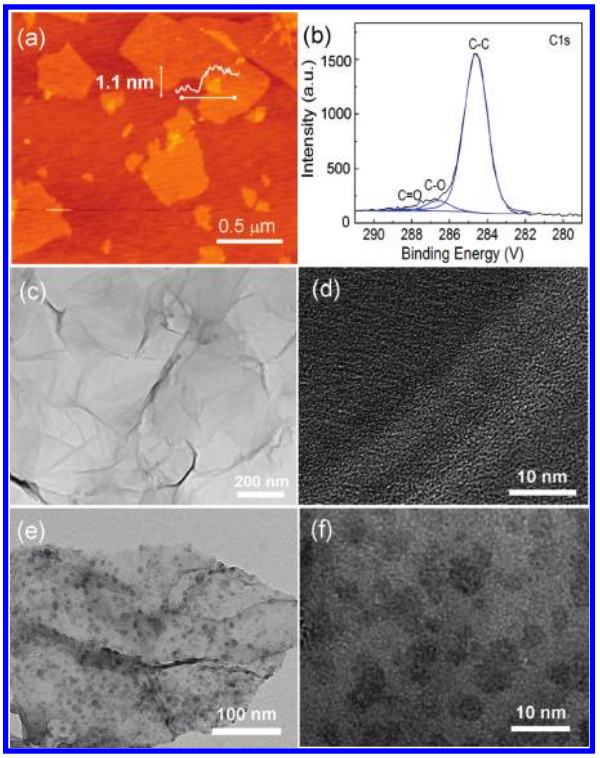

Figure 1. (a) AFM image of the as-prepared GO sheets. (b) high-resolution C1s XPS spectrum of graphene produced by chemical reduction of GO. TEM images of (c,d) the chemically reduced graphene and (e,f) the C_{60}-grafted graphene.

"clean" all-carbon hybrids for device applications. By using the resultant C_{60}−graphene hybrid as the electron acceptor in poly(3-hexylthiophene) (P3HT)-based bulk heterojunction solar cells, we demonstrated a 2.5-fold increase in the power conversion efficiency with an enhanced short-circuit current density and open-circuit voltage with respect to those of the C_{60}/P3HT system under AM 1.5 illumination (100 mW/cm^2).

In a typical experiment, graphene nanosheets were produced through reduction of GO (Figure 1a) in pure hydrazine according to the previously reported method.[27] The success of the chemical reduction of GO to graphene is evidenced by the high-resolution C1s X-ray photoelectron spectroscopic (XPS) result for the reduced graphene with a low percentage of C−O (286.5 eV) and C═O (288.1 eV) components, as shown in Figure 1b. Having been thoroughly dried in a vacuum oven at 80 °C, the as-prepared graphene nanosheets (5 mg) were then redispersed in dry toluene (10 mL) under nitrogen protection in a round-bottom flask. Thereafter, *n*-butyllithium in hexane (2.5 M, 0.8 mL) was added dropwise and kept sonication for 2 h. To the reaction mixture, 45 mg of C_{60} in toluene was added and the mixture was further sonicated for 3 h, followed by overnight stirring. Finally, a droplet of methanol (MeOH) was added to terminate the reaction. C_{60} residual, if any, was washed off with toluene followed by centrifugation. The resultant black solid was further purified by repeatedly rinsing with methanol and centrifugation. The resultant C_{60}-grafted graphene was then dried in vacuum at 60 °C overnight for subsequent characterization.

As demonstrated earlier with polydiene chains and CNTs,[24,25] the treatment of graphene with organolithium is expected to create a "living" center of lithium, where the nucleophilic addition of C_{60} takes place (Scheme 1). Subsequent termination with MeOH led to the formation of graphene grafted with methane-monosubstituted C_{60} buckyballs. However, chemically attached C_{60} moieties could form C_{60} clusters with free C_{60} molecules from solution as fullerene−C_{60} and its monosubstituted derivatives are susceptible to aggregation.[22,28,29]

Figure 1c,d shows transmission electron microscopic (TEM) images of the chemically reduced graphene under different magnifications. As can be seen, the graphene surface is smooth and free from any particulate contamination. By contrast, the corresponding TEM images for the C_{60}-grafted graphene under different magnifications given in Figure 1e,f clearly show a uniform surface grafted by particles with an average size of ∼5 nm characteristic of C_{60} aggregates.[28,29] The weight percentage of graphene in the C_{60}-grafted hybrids was determined by thermogravimetric analysis (TGA) to be ∼12%.

Further evidence for grafting C_{60} onto the graphene nanosheets comes from Fourier transform infrared (FTIR) and Raman spectroscopic measurements. As can be seen from Figure 2a, the grafting of C_{60} onto graphene nanosheets caused significant changes in the FTIR spectrum of the pure C_{60} or graphene. While a broad band similar to that of polyfullerene C_{60} clusters appeared at 1192 cm^{-1},[30] the band at 1385 cm^{-1} could be attributable to the characteristic IR mode of C_{60}, which is downshifted from 1428 cm^{-1}, presumably caused by the chemical modification and/or aggregation.[31,32]

Figure 2b shows Raman spectra of the pure C_{60}, the pristine graphene, the lithiated graphene prepared under nitrogen protection, and the C_{60}-grafted graphene. As expected, the chemically reduced graphene exhibits the D-band (sp^3 carbon) and G-band (sp^2 carbon) Raman peaks at 1357 and 1602 cm^{-1}, respectively,[33] while C_{60} shows the pentagonal pinch mode [$A_g(2)$] at 1466 cm^{-1} and additional H_g modes at 1425 and 1572 cm^{-1}.[34] For the C_{60}-grafted graphene, three Raman peaks are clearly observed at 1354, 1476, and 1601 cm^{-1}, which can be assigned to the D (1354 cm^{-1}) and G (1601 cm^{-1}) bands of the graphene and the $A_g(2)$ mode of C_{60}(1476 cm^{-1}) upshifted from the corresponding peak of the pure C_{60} at 1466 cm^{-1}. The observed peak shift implies the presence of a strong interaction

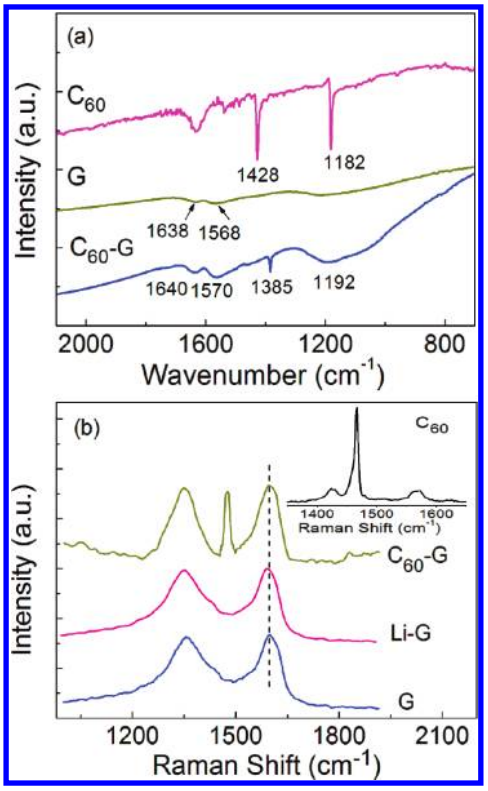

Figure 2. (a) FTIR and (b) Raman spectra of C_{60}, the chemically reduced graphene (G), the lithiated graphene (Li-G) prepared under nitrogen protection, and the C_{60}-grafted graphene (C_{60}-G). All the spectra have been randomly scaled along the *y*-axes for an easy comparison.

between the graphene sheets and C_{60}.[20] Additionally, it is noteworthy that the G band position for graphene (1602 cm^{-1}) downshifted to 1594 cm^{-1} (by 8 cm^{-1}) in the lithiated graphene, indicating the charge-transfer to the graphene framework from the lithium center.[26,35] By contrast, the G-band position for the C_{60}-grafted graphene shows an upshift by 7 cm^{-1} in comparison with the lithiated graphene, suggesting charge-transfer from the graphene network to the covalently bound C_{60}.[26] These results are consistent with the scenario schematically shown in Scheme 1. On the other hand, the D-band to G-band intensity ratio (I_D/I_G) has been widely used as a measure for the disorder or the extent of covalent modification of the graphene surface.[36] In particular, the grafting of C_{60} onto graphene should cause an increase in the I_D/I_G ratio. At first sight, the observed slight decrease in the I_D/I_G ratio from 0.98 for the graphene starting material to 0.91 for the C_{60}-grafted graphene in Figure 2b may appear surprising. However, it is important to notice that C_{60} was directly attached onto the graphene framework via monoaddition (Scheme 1). The monoaddition could have effectively extended, rather than disconnected, the sp^2 network of graphene over the chemically bound C_{60} moieties and the associated aggregates to decrease the I_D/I_G ratio, as shown in Figure 2b.

Recently, we have used P3HT-grafted graphene to significantly enhance the hole transport in a bilayer photovoltaic device, and hence the overall device performance.[10] Since graphene has been reported to show the highest room-temperature mobility for both hole and electron transport among all known carbon nanomaterials,[8] the newly synthesized C_{60}-grafted graphene (C_{60}-G) sheets are of great promise for polymer PVs. To demonstrate potential photovoltaic applications, we measured the optical absorption spectra of the C_{60}/P3HT and C_{60}-G/P3HT composite films spin-coated onto quartz plates. As can be seen in Figure 3a, both the C_{60}/P3HT and C_{60}-G/P3HT films exhibited two prominent absorption peaks; the broad absorption band over 500 nm corresponding to P3HT and the other at around 340 nm from C_{60}. Compared to the C_{60}/P3HT film, the P3HT absorption band for the C_{60}-G/P3HT film red-shifted by 18 nm with a concomitant increase in the absorption intensity over 500−650 nm, presumably due to the polymer chain alignment along the C_{60}-G surface.[37] Thermal annealing (130 °C, 10 min) of the C_{60}-G/P3HT film further enhanced the optical absorption over almost the entire visible region, while the P3HT absorption peak red-shifted from 518 to 530 nm (Figure 3a), indicating the formation of a more ordered polymer structure with additional advantages for the photovoltaic application.[38]

Using the C_{60}-G:P3HT (1:1 wt/wt), the C_{60}:P3HT (1:1 wt/wt), or the C_{60}/G mixture (i.e., 12 wt % graphene, physical blend without chemical functionalization):P3HT (1:1 wt/wt) as the active layer, we fabricated a series of bulk heterojunction solar cells with the structure of indium tin oxide (ITO)/poly-(3,4-ethylenedioxythiophene) (PEDOT):poly(styrenesulfonate) (PSS) (30 nm)/active layer (100 nm)/Al (100 nm) (Figure 3b). The parameters and current−voltage ($I-V$) characteristics for these solar cells with different active layers after annealing treatment (130 °C, 10 min) are shown in Figure 3c, while the corresponding numerical data are listed in Table 1. As shown in Figure 3c, an open-circuit voltage (V_{oc}) of 0.43 V, a short-circuit current (J_{sc}) of 2.34 mA/cm^2, and a power conversion efficiency (η) of 0.47% were obtained for the C_{60}:P3HT system under the illumination of AM 1.5 (100 mW/cm^2), while the C_{60}-G:P3HT system showed an η of 1.22% with a J_{sc} of 4.45 mA/cm^2 and a V_{oc} of 0.56 V. Clearly, therefore, the use of the C_{60}-grafted graphene as an electron acceptor in the photoactive layer improved the J_{sc} significantly without sacrificing the V_{oc}, yielding about 2.5-fold increase in the power conversion efficiency compared to the C_{60}:P3HT counterpart. The observed enhancement in J_{sc} could be attributed to the improved electron transport due to the presence of the C_{60}-grafted graphene. As is well-known, electrons can transport to the cathode only by hopping between C_{60} molecules in PVs with C_{60}:P3HT as the active layer. This would limit the charge collection efficiency because of possible charge recombination during the relatively slow hopping process. By contrast, the introduction of the C_{60}-grafted graphene could provide a direct conduction path for enhanced electron transport through a percolation of the highly conducting 2D graphene sheets throughout the composite layers. With a work function (−4.5 eV)[39] lower than the lowest unoccupied molecular orbital (LUMO) (−4.4 eV) of C_{60} and close to the work function of Al, graphene could act as an electron transport layer (ETL). As revealed by Figure 3d, electrons captured by C_{60} moieties could readily transfer to graphene and through its network to the Al cathode. This energetically favorable process for the C_{60}-G:P3HT PV should provide much more efficient electron transport than what could be obtained by the hopping process between C_{60} molecules in a C_{60}:P3HT device, though the energy barrier at the ETL/Al interface seems to be slightly higher for the former.

As a control, we also test the device performance using the C_{60}:graphene (12 wt % graphene) mixture with P3HT as the active layer fabricated in the same manner with identical structural parameters. In this case, the simple blending of C_{60} with graphene cannot ensure a good interfacial contact to facilitate strong electronic interactions for efficient electron transport

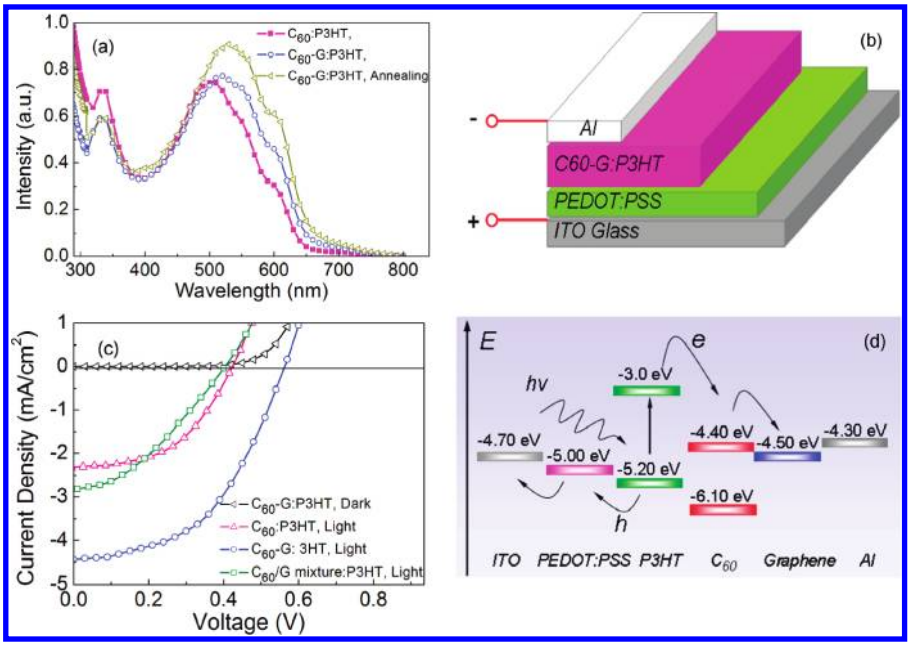

Figure 3. (a) Absorption spectra of the C_{60}-G:P3HT (1:1 wt/wt) film before and after annealing (130 °C, 10 min) and the C_{60}:P3HT (1:1 wt/wt) film spin-coated onto quartz plates. (b) Schematic of a hybrid photovoltaic device with the C_{60}-G:P3HT composite as the active layer. (c) $J-V$ curves of the photovoltaic devices with the C_{60}-G:P3HT (1:1 wt/wt), the C_{60}:P3HT (1:1 wt/wt), or the C_{60}/G mixture (12 wt % G):P3HT (1:1 wt/wt) as the active layers after annealing treatment (130 °C, 10 min). (d) Energy level diagram for the proposed photovoltaic device using the C_{60}-G:P3HT composite as the active layer.

Table 1. PV Characteristics (V_{oc}, J_{sc}, FF, and η) of the Devices with Different Active Layers

active layers	V_{oc} (V)	J_{sc} (mA cm^{-2})	FF	η (%)
C_{60}:P3HT	0.43	2.34	0.47	0.47
C_{60}-graphene:P3HT	0.56	4.45	0.49	1.22
C_{60}/graphene mixture:P3HT	0.40	2.81	0.39	0.44

between the two constituent components. To make it even worse, graphene sheets easily aggregated in the composite film, due to the poor miscibility, to show a detrimental effect on the charge separation/transport.[10] Therefore, the overall device efficiency was not remarkably improved (0.44%), despite the J_{sc} increasing slightly relative to its C_{60}:P3HT counterpart. Figure 4 shows atomic force microscopic (AFM) images of those different photoactive layers studied in this work. As can be seen, the blend film based on C_{60}:graphene mixture with P3HT has a surface root-mean-square roughness (Ra) of 9.7 nm, much higher than that of the C_{60}-G:P3HT blend film (Ra = 5.9 nm).[40] A rough surface morphology for the blend film could have led to a rough contact between the active layer and cathode, and hence the relatively poor device performance.[40]

Among all the photovoltaic devices studied in this work, the C_{60}-G:P3HT system shows the best overall device performance. The obtained power conversion efficiency for the ITO/PEDOT:PSS (30 nm)/C_{60}-G:P3HT(100 nm)/Al (100 nm) solar cell without optimization is much higher than those of similar polymer PVs containing a C_{60}−multiwalled carbon nanotube (MWCNT) complex (0.80%)[38] or a C_{60}−SWCNT complex (0.75%)[41] as electron acceptors and comparable to many high-performance PVs with nonfullerene electron acceptors.[39,42] Although the efficiency for the newly developed C_{60}-G:P3HT device (1.22%) is still relatively low compared to the widely investigated P3HT:phenyl-C_{61}-butyric acid methyl ester (PCBM) cells (5−6%),[43] the corresponding low fill factor (FF, Table 1) values suggested that there is still considerable room for future improvement in the device performance through optimization of the device structure.

In summary, we have developed a simple lithiation method for producing C_{60}-grafted graphene sheets. Detailed spectroscopic analyses confirmed that C_{60} molecules were covalently attached onto the graphene surface through monosubstitution. The resultant C_{60}-grafted graphene nanosheets have been used as electron acceptors in P3HT-based bulk heterojunction solar cells to significantly improve the electron transport, and hence the overall device performance. Without device optimization for the solar cell based on a C_{60}-grafted:P3HT active layer, we have demonstrated a 2.5-fold increase of the power conversion efficiency with an enhanced short-circuit current density and open-circuit voltage relative to those of its C_{60}:P3HT counterpart under AM 1.5 illumination (100 mW/cm^2). These results indicate that C_{60}-grafted graphene sheets are excellent electron accepting/charge transporting materials for constructing efficient polymer solar cells and for many other applications.

EXPERIMENTAL SECTION

Materials Preparation. GO powders were produced using a modified Hummers' method from graphite powder,[44] and graphene nanosheets were prepared through chemical reduction of the GO with hydrazine according to a reported procedure.[27] Briefly, 50 mg of GO was directly dispersed into 30 mL of 98% anhydrous hydrazine in a round-bottom flask at 98 °C in a nitrogen-filled drybox under stirring for 2 days. The resultant stable suspension was dried by thermal evaporation of the solvent.[27] For the preparation of C_{60}-grafted graphene, the dried graphene nanosheets (5 mg) were dispersed in dry toluene (10 mL) in a round-bottom flask under the protection of nitrogen

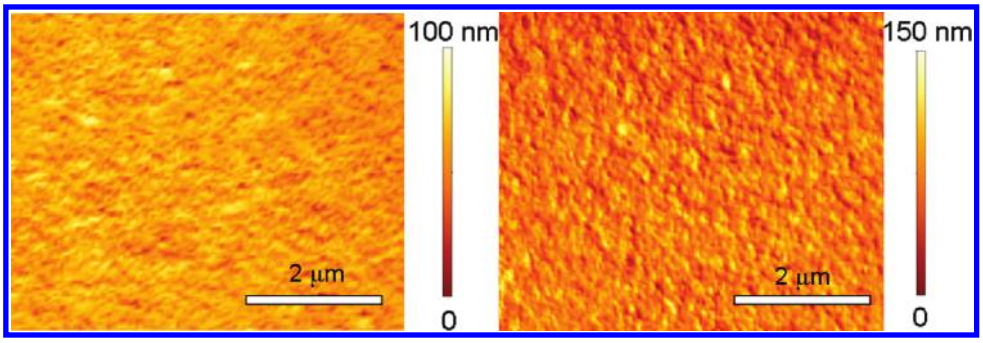

Figure 4. AFM images showing surface scan areas of (a) the C_{60}−G: P3HT film (Ra = 5.9 nm) and (b) the C_{60}:graphene mixture with P3HT film (Ra = 9.7 nm).

gas. Thereafter, *n*-butyllithium in hexane (2.5 M, 0.8 mL) was added dropwise and kept under sonication for 2 h. To the reaction mixture, 45 mg of C_{60} in toluene was then added and further sonicated for 3 h followed by overnight stirring. Finally, a droplet of methanol was added to terminate the reaction. The resultant C_{60}-grafted graphene was thoroughly washed with toluene and followed by centrifugation to remove C_{60} residual, if any. The final black powder was further rinsed with methanol, centrifuged repeatedly, and then dried in vacuum oven at 60 °C overnight.

Characterization. AFM (Micro 40, and Pacific Technology) was performed in the tapping mode while TEM images were recorded on a Hitachi H-7600 TEM unit (Hitachi, Japan). The surface chemistry was analyzed using a PHI Versa Probe XPS. FTIR spectra were recorded on a Perkin-Elmer FTIR spectrometer (Spectrum ONE). The Raman spectrum was recorded on a Renishaw inVia Raman spectrometer excited at 514.5 nm. UV−visible absorption spectra were recorded on a Perkin-Elmer Lambda 900 UV−vis−NIR spectrophotometer. TGA was carried out by a TA Instruments device with a heating rate of 10 °C in air.

Fabrication and Characterization of Photovoltaic Devices. Glass sheets coated with ITO were used as the substrate for device fabrication. The glass substrates were cleaned by consecutive sonication in detergent, deionized water, isoprophyl alcohol, and acetone in an ultrasonic bath, followed by UV-ozone cleaning (UVO-Cleaner, model no. 42, Jelight Company, Inc.) for 10 min. PEDOT:PSS (Bayton P, ∼30 nm in thickness) was spin-coated onto the clean substrate surface, followed by drying at 120 °C for 10 min to remove residual water. The photovoltaic active material of C_{60}/P3HT (1:1 wt/wt), C_{60}-G/P3HT (1:1 wt/wt) or C_{60}-G mixture (12 wt % G)/P3HT (1:1 wt/wt) in chlorobenzene solution (20 mg/mL) was then spin-coated on top of the PEDOT:PSS layer to produce an active layer of 100 nm, followed by annealing at 130 °C for 10 min, inside a N_2-filled glovebox. A 100-nm thick Al cathode was then vacuum-evaporated onto the photovoltaic active layer through a shadow mask to define an active area of 6 mm^2 for each device. The current−voltage (I−V) curves of the photovoltaic devices were recorded on a Keithly 236 source-measurement unit under simulated AM1.5 G irradiation (100 mW/cm^2), using a xenon lamp-based solar simulator (XPS-400, Solar Light Co.). All devices were fabricated and tested in an oxygen- and moisture-free nitrogen environment inside a glovebox.

AUTHOR INFORMATION

Corresponding Author

*E-mail: liming.dai@case.edu.

ACKNOWLEDGMENT

The authors acknowledge the support from AFOSR (FA9550-09-1-0331).

REFERENCES

(1) Novoselov, K. S.; Jiang, Z.; Zhang, Y.; Morozov, S. V.; Stormer, H. L.; Zeitler, U.; Maan, J. C.; Boebinger, G. S.; Kim, P.; Geim, A. K. Room-Temperature Quantum Hall Effect in Graphene. *Science* **2007**, *315*, 1379–1379.

(2) Stoller, M. D.; Park, S.; Zhu, Y.; An, J.; Ruoff, R. S. Graphene-Based Ultracapacitors. *Nano Lett.* **2008**, *8*, 3498–3502.

(3) Wang, X.; Li, X.; Zhang, L.; Yoon, Y.; Weber, P. K.; Wang, H.; Guo, J.; Dai, H. N-Doping of Graphene Through Electrothermal Reactions with Ammonia. *Science* **2009**, *324*, 768–771.

(4) Loh, K. P.; Bao, Q. L.; Eda, G.; Chhowalla, M. Graphene Oxide as a Chemically Tunable Platform for Optical Applications. *Nat. Chem.* **2010**, *2*, 1015–1024.

(5) Eda, G.; Fanchini, G.; Chhowalla, M. Large-Area Ultrathin Films of Reduced Graphene Oxide as a Transparent and Flexible Electronic Material. *Nat. Nanotechnol.* **2008**, *3*, 270–274.

(6) Yu, D. S.; Dai, L. M. Self-Assembled Graphene/Carbon Nanotube Hybrid Films for Supercapacitors. *J. Phys. Chem. Lett.* **2010**, *1*, 467–470.

(7) Wang, X.; Zhi, L. J.; Mullen, K. Graphene Electrodes for Dye-Sensitized Solar Cells. *Nano Lett.* **2008**, *8*, 323–327.

(8) Eda, G.; Chhowalla, M. Graphene-Based Composite Thin Films for Electronics. *Nano Lett.* **2009**, *9*, 814–818.

(9) Yu, D. S.; Dai, L. M. Voltage-Induced Incandescent Light Emission from Large-Area Graphene Films. *Appl. Phys. Lett.* **2010**, *96*, 143107(1−3).

(10) Yu, D. S.; Yang, Y.; Durstock, M.; Baek, J.-B.; Dai, L. M. Soluble P3HT-Grafted Graphene for Efficient Bilayer−Heterojunction Photovoltaic Devices. *ACS Nano* **2010**, *4*, 5633–5640.

(11) Gilje, S.; Song, H.; Wang, M.; Wang, K. L.; Kaner, R. B. A Chemical Route to Graphene for Device Applications. *Nano Lett.* **2007**, *7*, 3394–3398.

(12) Liu, Y.; Yu, D.; Zeng, C.; Miao, Z.; Dai, L. Biocompatible Graphene Oxide-Based Glucose Biosensors. *Langmuir* **2010**, *29*, 6158–6160.

(13) Qu, L.; Liu, Y.; Baek, J.; Dai, L. Nitrogen-Doped Graphene as Efficient Metal-Free Electrocatalyst for Oxygen Reduction in Fuel Cells. *ACS Nano* **2010**, *4*, 1321–1326.

(14) Paek, S.-M.; Yoo, E.; Honma, I. Enhanced Cyclic Performance and Lithium Storage Capacity of SnO_2/Graphene Nanoporous Electrodes with Three-Dimensionally Delaminated Flexible Structure. *Nano Lett.* **2009**, *9*, 72–75.

(15) Lu, J.; Do, I.; Drzal, L. T.; Worden, R. M.; Lee, I. Nanometal-Decorated Exfoliated Graphite Nanoplatelet Based Glucose Biosensors with High Sensitivity and Fast Response. *ACS Nano* **2008**, *2*, 1825–1832.

(16) Wudl, F. Fullerene Materials. *J. Mater. Chem.* **2002**, *12*, 1959–1963.
(17) Li, C.; Chen, Y.; Wang, Y.; Iqbal, Z.; Chhowalla, M.; Mitra, S. A Fullerene−Single Wall Carbon Nanotube Complex for Polymer Bulk Heterojunction Photovoltaic Cells. *J. Mater. Chem.* **2007**, *17*, 2406–2411.
(18) Liu, Z.; Liu, Q.; Huang, Yi.; Ma, Y.; Yin, S.; Zhang, X.; Sun, W.; Chen, Y. Organic Photovoltaic Devices Based on a Novel Acceptor Material: Graphene. *Adv. Mater.* **2008**, *20*, 3924–3930.
(19) Stankovich, S.; Dikin, D. A.; Dommett, G. H. B.; Kohlhaas, K. M.; Zimney, E. J.; Stach, E. A.; Piner, R. D.; Nyugen, S. T.; Ruoff, R. S. Graphene-Based Composite Materials. *Nature* **2006**, *442*, 282–286.
(20) Zhang, X.; Huang, Yi.; Wang, Y.; Ma, Y.; Liu, Z.; Chen, Y. Synthesis and Characterization of a Graphene−C_{60} Hybrid Material. *Carbon* **2009**, *47*, 334–337.
(21) Liu, Z.; Xu, Y.; Zhang, X. Y.; Zhang, X. L.; Chen, Y. S.; Tian, J. G. Porphyrin and Fullerene Covalently Functionalized Graphene Hybrid Materials with Large Nonlinear Optical Properties. *J. Phys. Chem. B* **2009**, *113*, 9681–9686.
(22) Dai, L. M. *Intelligent Macromolecules for Smart Devices: From Materials Synthesis to Device Applications*; Springer-Verlag: Berlin, 2004.
(23) Dai, L. M.; Albert, W. H.; Mau, H. J.; Griesser, T. S.; White, J. W. Grafting of Buckminsterfullerene onto Polydiene: A New Route to Fullerene-Containing Polymers. *J. Phys. Chem.* **1995**, *99*, 17302–17304.
(24) Dai, L. M.; Albert, W. H.; Mau, H. J.; Zhang, X. Synthesis of Fullerene- and Fullerol-Containing Polymers. *J. Mater. Chem.* **1998**, *8*, 325–330.
(25) Viswanathan, G.; Chakrapani, N.; Yang, H. C.; Wei, B. Q.; Chung, H. S.; Cho, K. W.; Ryu, C. Y.; Ajayan, P. M. Single-Step In Situ Synthesis of Polymer-Grafted Single-Wall Nanotube Composites. *J. Am. Chem. Soc.* **2003**, *125*, 9258–9259.
(26) Rodrigues, O. E. D.; Saraiva, G. D.; Nascimento, R. O.; Barros, E. B.; Mendes Filho, J.; Kim, Y. A.; Muramatsu, H.; Endo, M.; Terrones, M.; Dresselhaus, M. S.; Souza Filho, A. G. Synthesis and Characterization of Selenium Carbon Nanocables. *Nano Lett.* **2008**, *8*, 3651–3655.
(27) Tung, V. C.; Allen, M. J.; Yang, Y.; Kaner, R. B. High-Throughput Solution Processing of Large-Scale Graphene. *Nat. Nanotechnol.* **2009**, *4*, 25–29.
(28) Sun, N.; Wang, Y.; Song, Y.; Guo, Z.; Dai, L.; Zhu, D. Novel [60] Fullerene−Silver Nanocomposite with Large Optical Limiting Effect. *Chem. Phys. Lett.* **2001**, *344*, 277–282.
(29) Guo, Z.-X.; Sun, N.; Li, J.; Dai, L.; Zhu, D. Nanoscale Aggregation of Fullerene in Nafion Membrane. *Langmuir* **2002**, *18*, 9017–9021.
(30) Sun, Y. P.; Ma, B.; Bunker, C. E.; Liu, B. All-Carbon Polymers (Polyfullerenes) from Photochemical Reactions of Fullerene Clusters in Room-Temperature Solvent Mixtures. *J. Am. Chem. Soc.* **1995**, *117*, 12705–12711.
(31) Li, X.; Liu, L.; Qin, Y.; Wu, W.; Guo, Z. X.; Dai, L.; Zhu, D. C_{60} Modified Single-Walled Carbon Nanotubes. *Chem. Phys. Lett.* **2003**, *377*, 32–36.
(32) Zhang, H.; Fan, L.; Fang, Y.; Yang, S. Electrochemistry of Composite Films of C_{60} and Multiwalled Carbon Nanotubes: A Robust Conductive Matrix for the Fine Dispersion of Fullerenes. *Chem. Phys. Lett.* **2005**, *413*, 346–350.
(33) Kudin, K. N.; Ozbas, B.; Schniepp, H. C.; Prud'homme, R. K.; Aksay, I. A.; Car, R. Raman Spectra of Graphite Oxide and Functionalized Graphene Sheets. *Nano Lett.* **2008**, *8*, 36–41.
(34) Bethune, D. S.; Meijer, G.; Tang, W. C.; Rosen, H. J. The Vibrational Raman Spectra of Purified Solid Films of C_{60} and C_{70}. *Chem. Phys. Lett.* **1990**, *174*, 219–222.
(35) Wang, S.; Yu, D.; Dai, L. Polyelectrolyte Functionalized Carbon Nanotubes as Efficient Metal-Free Electrocatalysts for Oxygen Reduction. *J. Am. Chem. Soc.* **2011**, *133*, 5182–5185.
(36) Ferrari, A. C.; Meyer, J. C.; Scardaci, V.; Casiraghi, C.; Lazzeri, M.; Mauri, F.; Piscanec, S.; Jiang, D.; Novoselov, K. S.; Roth, S.;Raman Spectrum of Graphene and Graphene layers. *Phys. Rev. Lett.* **2006**, *97*, 187401(1−4).
(37) Berson, S.; Bettignies, R.; Bailly, S.; Guillerez, S.; Jousselme, B. Elaboration of P3HT/CNT/PCBM Composites for Organic Photovoltaic Cells. *Adv. Funct. Mater.* **2007**, *17*, 3363–3370.
(38) Li, C.; Chen, Y.; Ntim, S. A.; Mitraa, S. Fullerene−Multiwalled Carbon Nanotube Complexes for Bulk Heterojunction Photovoltaic Cells. *Appl. Phys. Lett.* **2010**, *96*, 143303(1−3).
(39) Liu, Q.; Liu, Z. F.; Zhang, X. Y.; Yang, L. Y.; Zhang, N.; Pan, G. P.; Yin, S. G.; Chen, Y. S.; Wei, J. Polymer Photovoltaic Cells Based on Solution-Processable Graphene and P3HT. *Adv. Funct. Mater.* **2009**, *19*, 894–904.
(40) Zhao, G.; He, Y.; Li, Y. 6.5% Efficiency of Polymer Solar Cells Based on Poly(3-hexylthiophene) and Indene-C_{60} Bisadduct by Device Optimization. *Adv. Mater.* **2010**, *22*, 4355–4358.
(41) Li, C.; Mitraa, S. Processing of Fullerene−Single Wall Carbon Nanotube Complex for Bulk Heterojunction Photovoltaic Cells. *Appl. Phys. Lett.* **2007**, *91*, 253112(1−3).
(42) Li, Y.; Hu, Y.; Zhao, Y.; Shi, G.; Deng, L.; Hou, Y.; Qu, L. An Electrochemical Avenue to Green-Luminescent Graphene Quantum Dots as Potential Electron-Acceptors for Photovoltaics. *Adv. Mater.* **2011**, *23*, 776–780.
(43) Brabec, C. J.; Gowrisanker, S.; Halls, J. J. M.; Laird, D.; Jia, S.; Williams, S. P. Polymer−Fullerene Bulk-Heterojunction Solar Cells. *Adv. Mater.* **2010**, *22*, 3839–3856.
(44) Becerril, H. A.; Mao, J.; Liu, Z.; Stoltenberg, R. M.; Bao, Z.; Chen, Y. Evaluation of Solution-Processed Reduced Graphene Oxide Films as Transparent Conductors. *ACS Nano* **2008**, *2*, 463–470.